Surface & Coatings Technology 228 (2013) 275–281

Contents lists available at SciVerse ScienceDirect

Surface & Coatings Technology

journal homepage: www.elsevier.com/locate/surfcoat

Microstructure, mechanical and tribological behaviors of MoS_2-Ti composite coatings deposited by a hybrid HIPIMS method

Xiaopeng Qin [a], Peiling Ke [a,*], Aiying Wang [a,*], Kwang Ho Kim [b]

[a] Ningbo Key Laboratory of Marine Protection Materials, Ningbo Institute of Materials Technology and Engineering, Chinese Academy of Sciences, Ningbo 315201, China
[b] National Core Research Center for Hybrid Materials Solution, Pusan National University, Pusan 609735, Korea

ARTICLE INFO

Article history:
Received 21 November 2012
Accepted in revised form 17 April 2013
Available online 24 April 2013

Keywords:
Hybrid high power impulse magnetron sputtering
MoS_2-Ti composite coatings
Microstructure
Tribology

ABSTRACT

The MoS_2-Ti composite coatings were deposited by a hybrid high power impulse magnetron sputtering (HIPIMS) source of Ti combined with a direct current magnetron sputtering (DC-MS) source of MoS_2. The composition, microstructure, mechanical and tribological behaviors of the MoS_2-Ti composite coatings were investigated using the various analytical techniques (XPS, SEM, XRD, TEM, nano-indentation, scratch and ball-on-disk test). The results showed that doping Ti using HIPIMS technique enabled MoS_2 coatings to grow in the form of a dense amorphous structure. The crystallization degree of the MoS_2-Ti composite coatings decreased with the increase of doped titanium content. Ti reacting with O to form titanium oxides in the surface inhibited the oxidation of MoS_2. The hardness and adhesion of the composite coatings reached its maximum within a certain range of Ti content. Doped Ti improved the tribological properties of pure MoS_2 coatings in the atmospheric environment. The coefficient of friction (COF) decreased with the increase of Ti content. The lowest average COF at 0.04 and the wear rate at 10^{-7} mm^3 N^{-1} m^{-1} were achieved at the optimum of Ti content at 13.5 at.%. The improved tribological property was discussed in terms of the obtained higher hardness and better adhesion of the composite coatings combined with inhibition of MoS_2 oxidation.

1. Introduction

Sputtered MoS_2 coating as an excellent solid lubricant has been widely used in the vacuum and space field such as the spacecraft motion components and rolling bearings due to the high wear resistance durability and very low coefficient of friction [1,2]. However, pure sputtered MoS_2 coating generally exhibits the loose structure, low hardness and high chemical activity to oxygen, resulting in the deteriorated wear durability and the corrosion resistance [3]. Recently, doping small amount of metal or ceramic elements into MoS_2 coatings has been attempted to improve the lubricant and corrosion performance of MoS_2 coating [4–9]. It is found that doping the metals such as Al, Au, W, etc., in the MoS_2 coatings by magnetron co-sputtering showed good friction stability in ambient air with long-lasting wear durability [5–7]. In addition, introduction of TiN or TiB_2 was also developed to modify the tribological properties of pure MoS_2 coatings [10,11]. Specially, note that the addition of Ti into the MoS_2 coating in recent years has drawn much attention because of the significant improvement of the oxidation resistance and tribological performance dependent on the humidity in ambient air [12].

Usually, the employed doping metal components are acquired using a conventional direct current magnetron sputtering. However, the ionization degree of the plasma particles is relatively low, leading to poor coating adhesion to substrate and densification deterioration of coating structure [12,13]. As a consequence, the coating was suffered from the structural degradation due to oxidation causing lubrication failure.

A magnetron sputtering method, which is called high power impulse magnetron sputtering (HIPIMS), has been developed since 1990s, where high density plasma with electron densities about 2–3 orders of magnitude larger than those obtained in conventional magnetron sputtering and high sputtering particle ionization rate may be achieved [14–16]. A great deal of research has been conducted to study the effects of this technique on properties of the deposited coating [17,18], such as densification, changes in structure and properties of coating [19]. From a durability and reliability prospective of MoS_2 coatings in multi-environmental application, if the HIPIMS technique as a metal plasma source is combined with the deposition of MoS_2 coatings, rather than the general used DC-MS and cathodic arc plating hybrid method, one can expect that the structure and properties of coating could be well tailored according to the demanded applications [19].

HIPIMS requires higher excitation voltage, then the ionized particles may be draw back by target itself because of the high negative voltage of the target surface, causing low film deposition rate. To solve the problem, a modified HIPIMS power supply coupled a DC unit with the high power pulse unit has been employed in the

* Corresponding authors. Tel.: +86 574 86685036.
E-mail addresses: kepl@nimte.ac.cn (P. Ke), aywang@nimte.ac.cn (A. Wang).

0257-8972/$ – see front matter © 2013 Elsevier B.V. All rights reserved.
http://dx.doi.org/10.1016/j.surfcoat.2013.04.040

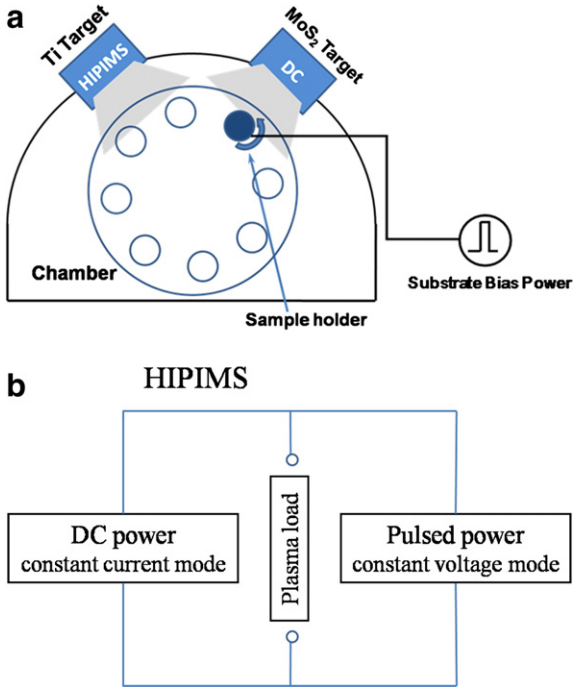

Fig. 1. Schematic diagrams: (a) the hybrid HIPIMS deposition system of MoS_2-Ti composite coatings and (b) a parallel connection operation mode of HIPIMS power supply.

present work. On the one hand, a high deposition rate can be obtained by the coupled DC unit; on the other hand, a DC unit could optimize pulse glowing and plasma stabilization through pre-ionization [11,20]. During the deposition, the power supply was able to deliver both pulses and DC, where a DC unit was also used to easily control the doped Ti content in the coatings. In addition, a high power impulse could produce plasmas with highly ionized metallic species with high ion energy. In the preliminary research work, we obtained the optimized parameters of high power pulse part, pressure and bias voltage, which were fixed in the process and were beneficial to enhanced mechanical and tribological behaviors of MoS_2-Ti composite coatings.

MoS_2-Ti composite coatings with different Ti contents were thereafter deposited by the co-sputtering of the hybrid HIPIMS system for Ti and a DC magnetron sputtering unit for MoS_2. Different Ti doping contents in the coatings were obtained by varying the target current. The influence of Ti contents on microstructure, mechanical properties and tribological behaviors in atmospheric environment was investigated.

2. Experimental details

Hybrid high power impulse magnetron sputtering system was employed to deposit the pure MoS_2 and MoS_2-Ti composite coatings onto mirror-finished high speed steel (HSS) discs and silicon P-(100) substrates. The system was combined with a Ti target connecting to high power impulse power supply with a MoS_2 target connecting to DC power supply. The distance between the target and the substrate was 11 cm. The schematic diagram of the system is shown in Fig. 1(a), and the parallel connection of HIPIMS power supply is shown in Fig. 1(b), in which the pulsed power by the constant voltage mode is adjusted to achieve the high impulse power and the DC power by the constant current mode was regulated to obtain the different content of doped Ti. Before loading into the vacuum chamber, all the substrates were ultrasonically cleaned in acetone and ethanol for 15 min, respectively, and then dried in air. Thereafter, the cleaned substrates were mounted on the rotated substrate holder in the chamber. Prior to deposition, the chamber was pumped down to less than 3×10^{-5} Torr, and the substrates were cleaned in the argon plasma for 30 minutes. The Ti interlayer (~100 nm) was first constructed to enhance the coating adhesion to the substrate. During the deposition of top MoS_2-Ti composite coatings, DC magnetron sputtering current applied onto the MoS_2 target was fixed at 1.0 A, and HIPIMS power with various currents (0.5, 0.8, 1.0, 1.5 and 2.0 A) was supplied to the Ti target magnetron sputtering unit to control the doped Ti content in the coatings. The process parameters are shown in Table 1. A negative pulsed direct current bias, with a frequency of 350 kHz and reverse time of 1.1 μs, was applied to the substrates during the coating deposition.

The thicknesses of the deposited coatings were measured by a surface profilometer (KLA-Tencor, Alpha-Step IQ) through a step between the coatings and the Si wafers covered with a shadow mask. Surface morphology of the coatings was studied by a field emission scanning electron microscope (S4800, Hitachi). The composition and chemical bonds of the deposited coatings was analyzed by X-ray photoelectron spectroscopy (XPS, Axis ultraDLD) with Al (mono) Kα irradiation at the pass energy of 160 eV. Before taking the measurement, an Ar + ion beam with the energy of 3 keV was used to etch the sample surface for 5 min to remove contaminants. X-ray diffraction (XRD) measurements were performed by AXS D8 Advance diffractometer (Bruker). High-resolution transmission electron microscopy (TEM) of the coatings was carried out on a Tecnai F20 electron microscope (FEI), which was operated at 200 KeV with a point-to-point resolution of 0.24 nm. The specimens for TEM analysis, with thicknesses of about 50 nm, were deposited directly on freshly cleaved single-crystal NaCl wafers and then were peeled off through dissolving the NaCl wafers in the deionized water.

Mechanical properties of the coatings were tested by the nano-indentation technique (MTS NANO G200) in a continuous stiffness measurement mode using a Berkovich diamond tip. The characteristic hardness was chosen in a depth of around 1/10 of the coating thickness where the contribution of Si substrate to the results could be ignored. The adhesion of the coatings on the HSS substrate was performed by a CSM scratch tester with a Rockwell-G diamond

Table 1
Process parameters for MoS_2-Ti composite coatings deposition.

Deposition parameters	Ti interlayer	MoS_2-Ti composite coatings
Ar (sccm)	40	50
Bias voltage (V)	−100	−300
Pulse width (μs)	100	100
Pulse frequency (Hz)	100	100
Ti target pulse voltage (V)	500	500
Ti target direct current (A)	2.0	0.5, 0.8, 1.0, 1.5, 2.0

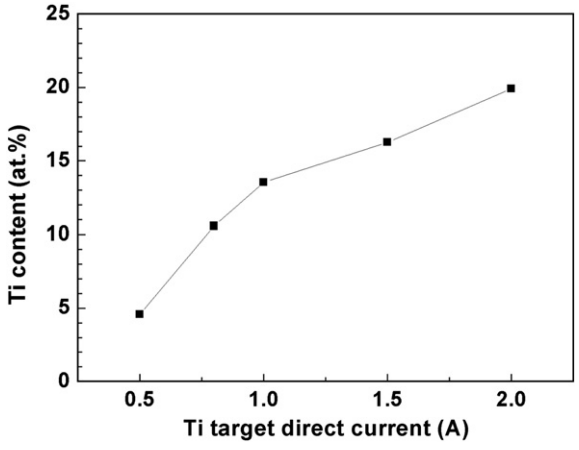

Fig. 2. Ti content of MoS_2-Ti composite coatings with different Ti target direct currents.

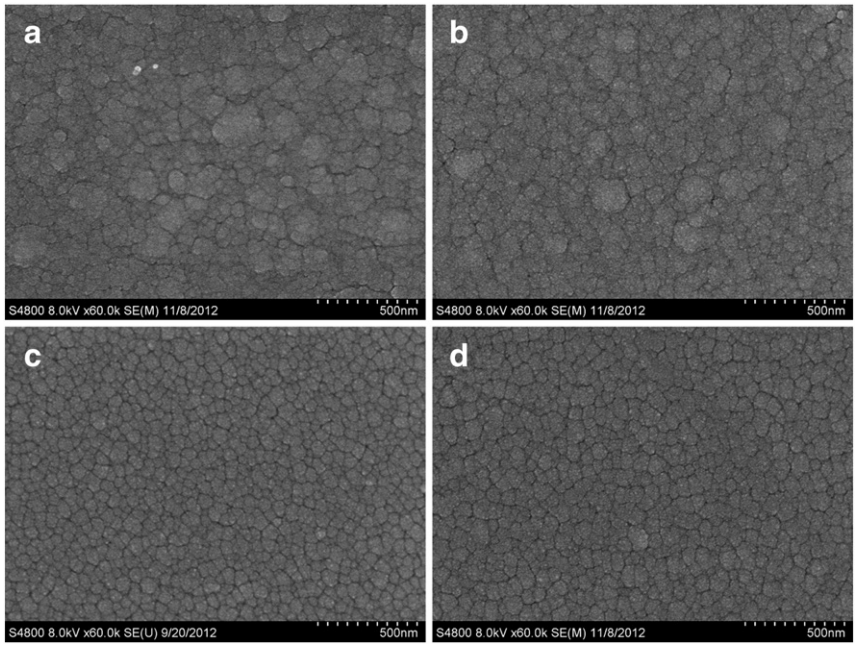

Fig. 3. Surface SEM images of MoS_2-Ti composite coatings with different Ti contents at (a) 0 at.%, (b) 4.6 at.%, (c) 13.5 at.% and (d) 19.9 at.%.

indenter (200 μm tip radius) at a constant sliding speed of 6 mm/min and a scratch length of 3 mm. The normal load increased linearly to 60 N (the maximum load was 20 N for the pure MoS_2 coating). The critical loads at which the films were delaminated from the substrate with the thinning deformation of the film were usually assessed as a criterion of the adhesive strength. Two to three tests were done on each sample to confirm the critical load. The tribological behavior of coatings deposited on the HSS discs was tested by a rotary ball-on-disk tribometer (JLTB-02) at room temperature with a relative humidity of about 70%. A steel ball (SUJ-2, HRC60) with a diameter at 6 mm was used as the friction counter ball. All the tests were performed at 0.2 m/s sliding velocity for a maximum distance of 500 m, and the applied load was 3 N.

3. Results and discussion

Fig. 2 shows the Ti content in the deposited MoS_2-Ti coatings as a function of the Ti target direct current. With the increase of the Ti target direct current, the Ti content in the coatings increased monotonically. As the current increased from 0.5 to 2.0 A, the Ti content was found increasing from 4.6 to 19.9 at.%. This indicates that the Ti content in the coatings could be well controlled by adjusting the Ti target direct current in the hybrid HIPIMS system.

Fig. 3 shows SEM images of the surface morphology for MoS_2-Ti composite coatings with different Ti contents. For the pure MoS_2 without Ti doping, as shown in Fig. 3(a), the surface revealed a loose and granular structure, where the gaps between agglomerated grains were visible. Doping Ti leaded to the densification and compaction of the coating, displaying a dense structure, as evidently demonstrated in Fig. 3(b) and (c). As the Ti content increased, the grain size in the surface decreased, and the dense dome structure in the surface of the coating emerged. Considering of the observed increase of hardness with increasing the Ti content reported elsewhere [11,21], it could be deduced that the structure densification caused by the doped Ti would improve the mechanical property and oxidation resistance in humid environment of the MoS_2 coating. Further increase in Ti content to 19.9 at.% led the grains to expand as revealed from Fig. 3(d), which may cause decreased mechanical properties of the coating.

The chemical bonds of the deposited MoS_2-Ti coatings with different Ti contents were characterized by the XPS spectra as shown in Fig. 4. In order to further justify the chemical forms of Mo, S and Ti in the coatings, the Mo 3d, S 2p and Ti 2p spectrum of the typical coating with the Ti content at 13.5 at.% is fitted by Guassian–Lorentian function (GL30), as shown in Fig. 5. The Mo 3d spectrum for all the samples shows a small shoulder peak at around 226 eV binding energy, which is identified as the S 2s peak. The Mo 3d spectrum (Fig. 4a) at the binding energy of 228.8 and 231.9 eV corresponds to the standard spectral line of Mo $3d_{5/2}$ and Mo $3d_{3/2}$in MoS_2 (Mo^{4+}), respectively [22,23]. However, there is another Mo 3d doublet in the deconvolution of the Mo 3d spectrum shown in Fig. 5a. The peaks at 228.1 and 231.2 eV are consistent with the Mo $3d_{5/2}$ and Mo $3d_{3/2}$ in MoS. For the pure MoS_2 coating, there is a peak at higher binding energy with Mo $3d_{3/2}$ at 235.6 eV shows the existence of Mo-O bonds (Mo^{6+}) [24]. The S 2p spectrum (Fig. 4b) shows a doublet at binding energy of 162.1 and 163.3 eV, which represents the S $2p_{3/2}$ and S $2p_{1/2}$ spectral lines of S^{2-} in MoS_2, but S/Mo does not match the stoichiometric ratio of 2:1. The deconvolution of the S 2p spectrum in Fig. 5b reveals that the S 2p peaks at 161.5 and 162.7 eV are identified corresponding to the standard S $2p_{3/2}$ and S $2p_{1/2}$ lines in MoS, which is in good agreement with the analysis on the Mo 3d spectrum [22,23,25]. It can be concluded that both MoS_2 and MoS exist in the composite coatings, and that the ratio of S to Mo is lower than 2, about 1.4 by XPS. In the Ti 2p spectrum (Fig. 4c), there is a slight increasing of the intensity occurred with the increase of Ti content within the coating. The deconvolution of the Ti 2p spectrum in Fig. 5c shows that the obvious Ti 2p peaks at 457.5 and 463 eV correspond to Ti $2p_{3/2}$ and Ti $2p_{1/2}$ in TiO_2, and other two peaks correspond to the standard Ti $2p_{3/2}$ (455.2 eV) and Ti $2p_{1/2}$ (460.7 eV) in Ti_2O_3, respectively [22]. Detailed XPS line positions and chemical state assignments can be seen in Table 2 [22,23]. In our case of the MoS_2-Ti composite coatings, the Mo-O bond was invisible from the XPS spectrum. Instead, there were more obvious Ti-O bonds with the increase of the incorporation of Ti, implying that the doped Ti combining with O formed the titanium oxides in the surface. As a consequence, the oxidation of MoS_2 was inhibited to a great extent.

Fig. 6 shows the crystallinity evolution of the coatings as a function of the Ti contents measured by the XRD spectra. Besides the diffraction peak arisen from the Si substrate (marked as Si in

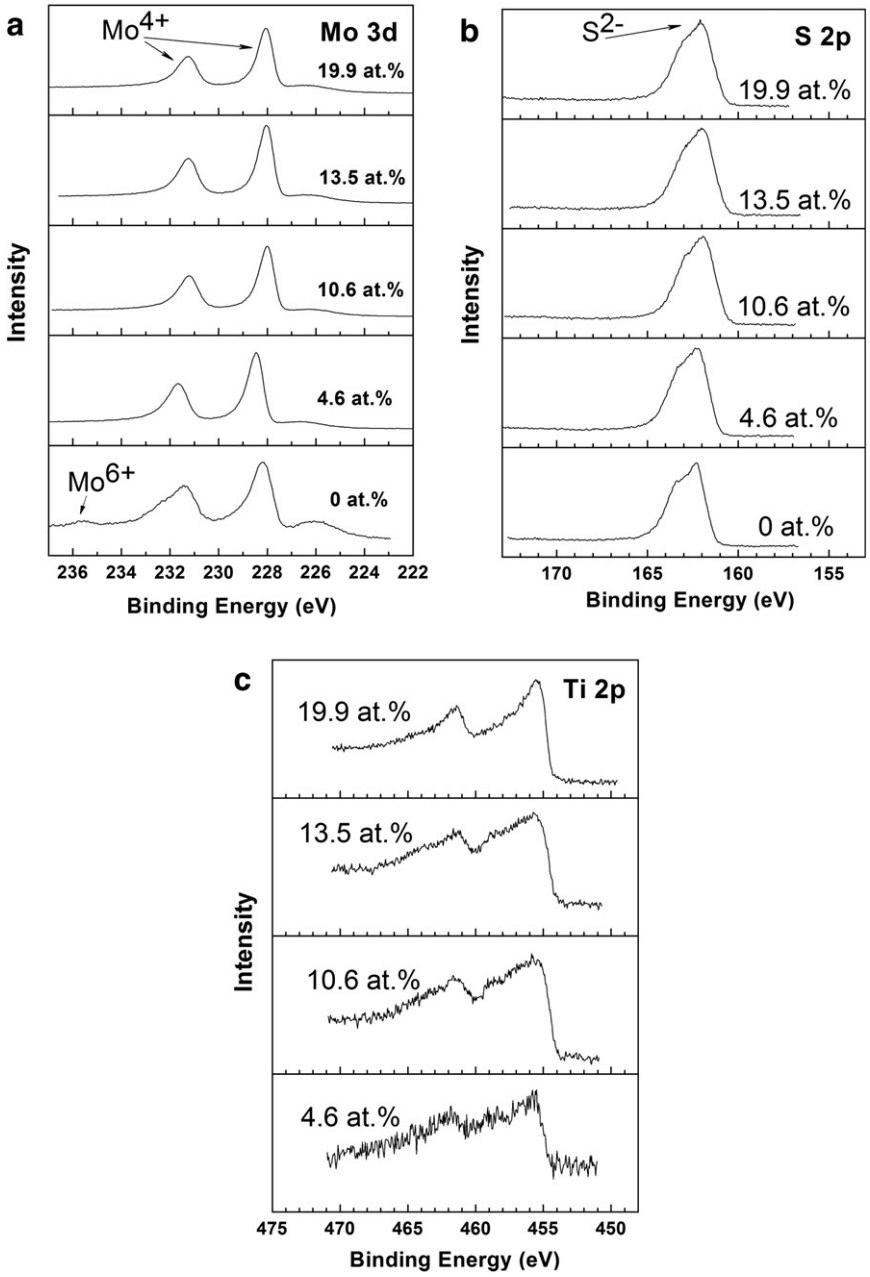

Fig. 4. XPS spectrums of MoS_2-Ti composite coatings with different Ti contents: (a) Mo 3d, (b) S 2p and (c) Ti 2p.

the figure), there was an evident peak at around 2θ from 10° to 15° for the pure MoS_2 coating (without Ti incorporation in the top layer), which was assigned to the MoS_2 (002) plane. The intensity of MoS_2 (002) diffraction peak was weakened and gradually disappeared with the increase of the doped Ti content. The degree of crystallization of the MoS_2-Ti composite coatings decreased with the increase of Ti content, and the structure of the MoS_2-Ti composite coatings turned into the possible dominated amorphous structure. The phenomena could be attributed to the lattice distortion caused by the incorporation of Ti [26]. Meanwhile, the peaks at around $2\theta = 38°$ was visible in the obtained XRD spectra, assigned to the Ti diffraction peak, which was likely to have resulted from the Ti interlayer or the top composite coating.

In order to further clarify the cause of observed Ti diffraction peak, TEM characterization was carried out. The specimen with thicknesses of about 50 nm was deposited directly on freshly cleaved single-crystal NaCl wafers using the DC magnetron sputtering with the MoS_2 target current at 1.0 A and the Ti target HIPIMS pulse currents at 1.0 A. After deposition, the coating was peeled off through dissolving the NaCl wafers in the deionized water. Fig. 7 shows the representative TEM micrograph and the corresponding selected area electron diffraction (SAED) pattern of the coating with 13.5 at.% Ti. The SAED showed the broad and diffuse halo diffraction, which was almost the typical amorphous feature. Comparing with the results shown in Fig. 6, this confirmed that the top MoS_2-Ti composite coating essentially was in the state of typical amorphous structure. As a result, the Ti diffraction peak in XRD spectra was deduced resulting from the Ti interlayer, which was in good consistency with the analysis in Fig. 6.

The hardness of the MoS_2-Ti composite coatings as a function of the Ti content is given in Table 3. Within the current lower Ti content region of 0–13.5 at.%, increasing the Ti content led to the significant increase of the hardness of the coatings. For the pure MoS_2 coating, the hardness was only about 3.33 GPa, while it increased to 9.69 GPa with the Ti content of 13.5 at.%, which was almost three times larger than that of pure MoS_2. However, further increasing

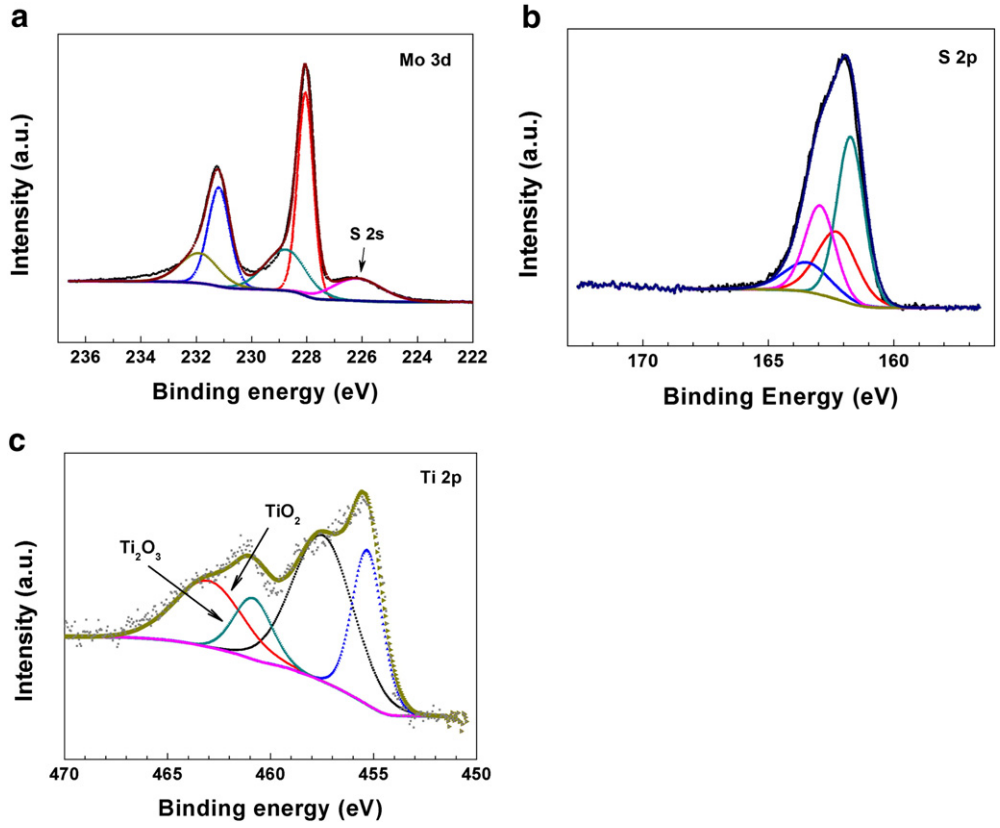

Fig. 5. Decomposition of the Mo 3d (a), S 2p (b) and Ti 2p (c) spectral region of the typical coating with the 13.5 at.% Ti.

Ti content to 19.9 at.% caused the hardness decrease to 6.82 GPa. Taking into account the structure densification dependence on the Ti content, the hardness increase of the MoS_2-Ti composite coating could be understood by the solid solution hardening effect [7]. In this case, the hardness firstly increased and reached to the maximum value due to the structure densification with a certain of saturation value of Ti content. Beyond of this threshold value of 13.5 at.% Ti, the overrich doped soft Ti atoms in turn caused the structure deterioration and led to the decrease of hardness. Similar results could be found in the other study of MoS_2-Ti composite coating [4,26].

To obtain the high adhesion is one of the major technology challenges for sputtered MoS_2 solid lubricating coatings on bearing steel, which play the crucial role on the tribological property of the coating. Table 3 shows the critical loads of the pure MoS_2 and MoS_2-Ti composite coatings on HSS substrate. The results showed that all the MoS_2-Ti composite coatings with different Ti content owned much higher critical load than the pure MoS_2 coating, and within the lower Ti content region of 0–13.5 at.%, increasing the doped Ti content led to the significant increase of the critical load of the coatings. It can be deduced that Ti concentration seemed to play a considerable role in coating adhesion. Previous studies [27] indicated that adhesion failure mechanisms displayed the film cohesion failure at the beginning, followed by spalling between coating and buffer, then substrate. This improvement in coating adhesion with increase in Ti content maybe attributed to the bombardment of more high-energy Ti particles, resulting in enhanced densification and cohesion of the coating. There was also interdiffusion between MoS_2-Ti composite layer and Ti interlayer deposited at the initial stage of coating preparation. The more bombardment by Ti particles provided better bonding between coating and buffer and better adhesion [28]. It can be observed that maximum coating adhesion was obtained with a critical load of 58 N for the 13.5 at.% Ti content, consistent with the results of hardness. The previous research by Bidev and Holmberg [29,30] showed that the adhesion intensified with the increase of film hardness. Thence, the critical

Table 2
XPS line positions and chemical state assignments.

Line	Position (eV)	Assignment
Mo $3d_{5/2}$	228.8	MoS_2
	228.1	MoS
S $2p_{3/2}$	162.1	MoS_2
	161.5	MoS
Ti $2p_{3/2}$	457.5	TiO_2
	455.2	Ti_2O_3

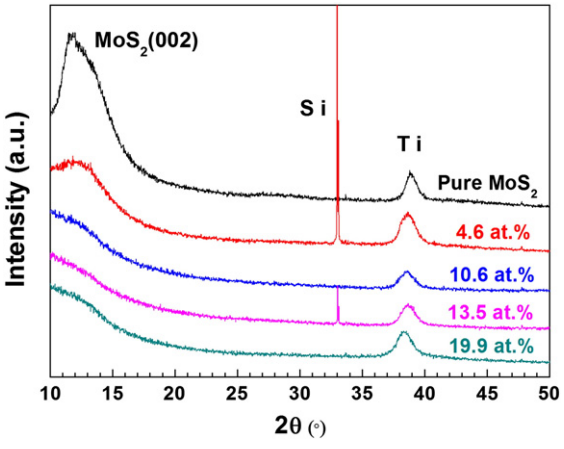

Fig. 6. XRD spectra of MoS_2-Ti composite coatings.

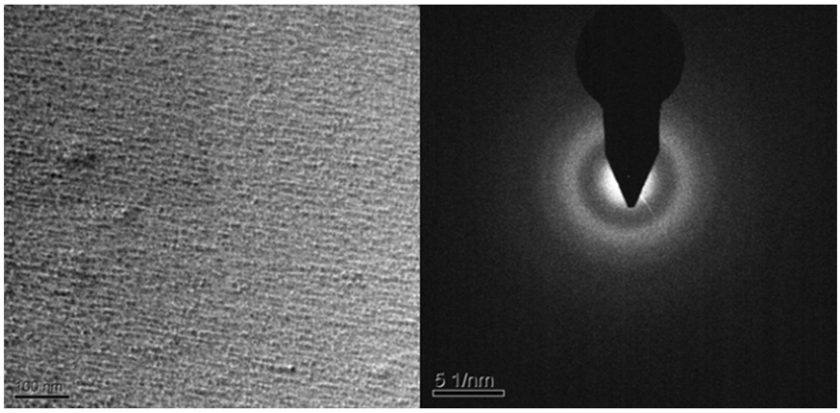

Fig. 7. TEM images of MoS_2-Ti composite coating with 13.5 at.% Ti.

loads of the coatings that were consistent with the results of hardness correspond to the conclusions in literature. However, further increasing Ti content to 19.9 at.% caused the densification deterioration of the coating, thus lowering the coating hardness and adhesion.

In order to investigate the effect of doped Ti content on the tribological behavior of the MoS_2-Ti composite coatings, ball-on-disk friction tests were performed under ambient air against steel balls. Fig. 8(a) shows the friction coefficient of the coatings as a function of the sliding distance. For the pure MoS_2 coating, the friction coefficient kept in the relative steady state within the first sliding period and rose sharply at the distance of about 100 m, implying the lubrication failure in humid atmospheric environment and a poor wear durability. Meanwhile, the friction showed a significant fluctuation and unsteady state. However, doping the Ti into the coatings containing some Ti content (<15 at.%) presented a relatively steady and low friction coefficient lower than the pure MoS_2. It indicated that the doped Ti improved the tribological properties of pure MoS_2 in the atmospheric environment. Fig. 8(b) shows that with the increase of the Ti content, the average friction coefficient of the coating reduced from 0.24 (pure MoS_2) to 0.04 (MoS_2-Ti, 13.5 at.% Ti). In some literature [9,11], the gradual optimization of tribological properties is due to the increase of both hardness and adhesion of the MoS_2-Ti coatings. Therefore, the highest coating hardness and best adhesion together with dense structure for the MoS_2-Ti composite coating with 13.5 at.% Ti content may account for its best tribological behavior. In addition, during wear, MoS_2 could be oxidized into MoO_3, directly causing an abrasive effect as an anti-lubricating component [31]. The formation of oxidation products led to an increase of CoF and decrease of wear life, thus creating a corrosive and abrasive effect on the contrary. Based on the XPS analysis of the MoS_2-Ti composite coatings, the incorporation of titanium can protect MoS_2 structure from oxygen contamination. The presence of the titanium atoms within the MoS_2 structure prevented the erosion of the water vapor and oxygen. With the increase of the Ti content, more MoS_2 was protected, and less formation of MoO_3 existed. Hence, the coatings are more resistant to the effects of humid air and maintain the lower CoF. However, further increasing the Ti content, the friction coefficient of the coatings increased with a short wear life due to its lower hardness and poor adhesion. Similar results were also reported in earlier literature [32].

It is well know that the MoS_2 layer is easy to slide due to its low shear force in a tangential direction [1], but the loose structure is prone to water adsorption and easily oxidized in humid atmospheric environment, causing an increase of friction coefficient and a decrease of coating friction lifetime [3]. Appropriate doped Ti led to high coating adhesion and hardness combined with the densification

Table 3
Hardness and adhesion test results of MoS_2-Ti composite coatings with different Ti contents.

Ti content (at.%)	Hardness (GPa)	Critical load (N)
0	3.33	3
4.6	5.21	21
10.6	6.82	29
13.5	9.69	58
19.9	6.82	12

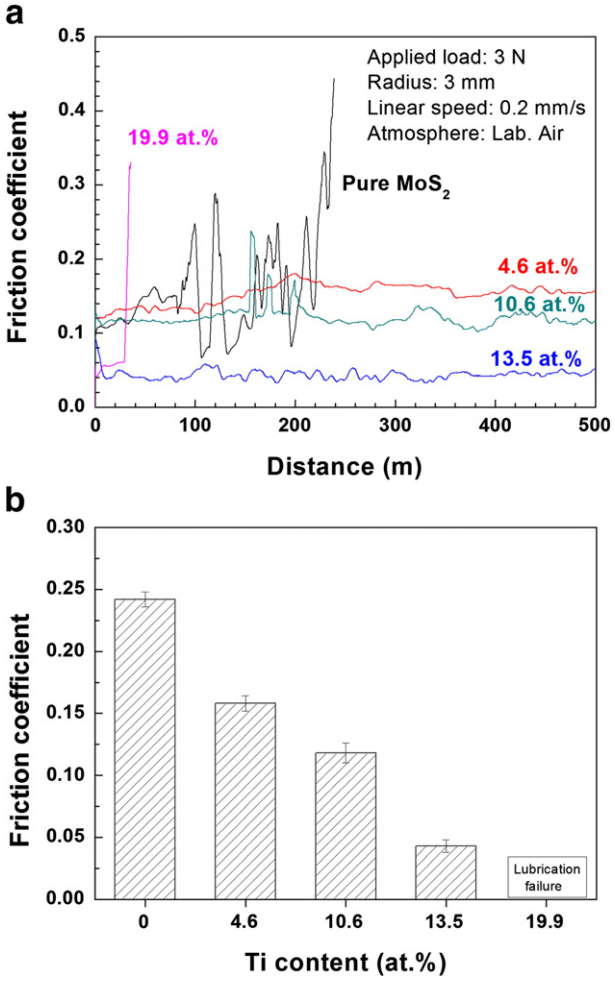

Fig. 8. (a) Sliding friction curves and (b) average friction coefficient of MoS_2-Ti composite coatings with different Ti contents.

and compaction of the coating, which benefited sliding possible with a extremely low friction coefficient and the improved endurance in sliding contacts even under humid atmospheric environment [6,12,33]. In addition, the formation of titanium oxides in surface of the coating could effectively prevent the oxidation of MoS_2, thus improving the wear life of the coating.

4. Conclusions

MoS_2-Ti composite coatings with Ti contents varying from 0 to 19.9 at.% were deposited by a hybrid HIPIMS system comprising of a DC magnetron sputtering source and a HIPIMS source. Doping Ti into MoS_2 coating led to the emergence of structure densification. With the increase of Ti content, the phase crystallinity of the MoS_2-Ti composite coatings decreased, and the increased amorphous structure played great role to the coating performance. The results showed that both the mechanical and the tribological behavior of the coating were significantly improved as the Ti was doped into the sputtered MoS_2 coatings. Note that the maximum hardness and adhesion were found with the Ti content of 13.5 at.% of the MoS_2-Ti composite coatings. Meanwhile, coatings with approximately doped 13.5 at.% Ti displayed the excellent lubricant and wear resistant performance, where the friction coefficient showed the very steady state behavior and the lowest average value of 0.04. The higher coating hardness and better adhesion had vital influences on the tribological property of the composite coatings. The present results provide us the effective way to modify the tribology behavior of pure MoS_2 coating and realize its widely industrial applications as solid lubricants with high performance.

Acknowledgments

This work was financially supported by the programs of the State Key Project of Fundamental Research of China (grant no. 2013CB632302), the National Nature Science Foundation of China (grant no. 51005226) and the Ningbo Municipal Government (grant nos. 2011B1016, 2010D10015 and 2011B81001).

References

[1] T. Spalvins, ASLE Trans. 12 (1969) 36.
[2] C. Donnet, A. Erdemir, Tribol. Lett. 17 (2004) 389.
[3] D.Y. Wang, C.L. Chang, Z.Y. Chen, W.Y. Ho, Surf. Coat. Technol. 120 (1999) 629.
[4] J.R. Lince, M.R. Hilton, A.S. Bommannavar, J. Mater. Res. 10 (1995) 2091.
[5] M.C. Simmonds, A. Savan, E. Pflüger, H. Van Swygenhoven, Surf. Coat. Technol. 126 (2000) 15.
[6] J.J. Nainaparampil, A.R. Phani, J.E. Krzanowski, J.S. Zabinski, Surf. Coat. Technol. 187 (2004) 326.
[7] N.M. Renevier, V.C. Fox, D.G. Teer, J. Hampshire, Surf. Coat. Technol. 127 (2000) 24.
[8] H. Du, C. Sun, W. Hua, T. Wang, J. Gong, X. Jiang, S.W. Lee, Mater. Sci. Eng. A Struct. 445–446 (2007) 122.
[9] X. Wang, Y. Xing, S. Ma, X. Zhang, K. Xu, D.G. Teer, Surf. Coat. Technol. 201 (2007) 5290.
[10] M. Steinmann, A. Müller, H. Meerkamm, Tribol. Int. 37 (2004) 879.
[11] S. Gangopadhyay, R. Acharya, A.K. Chattopadhyay, S. Paul, Surf. Coat. Technol. 203 (2009) 1565.
[12] N.M. Renevier, J. Hamphire, V.C. Fox, J. Witts, T. Allen, D.G. Teer, Surf. Coat. Technol. 142 (2001) 67.
[13] J.W. Bradley, S. Thompson, Y.A. Gonzalvo, Plasma Sources Sci. Technol. 10 (2001) 490.
[14] V. Kouznetsov, K. Macak, J.M. Schneider, U. Helmersson, I. Petrov, Surf. Coat. Technol. 122 (1999) 290.
[15] J. Bohlmark, J. Alami, C. Christou, A.P. Ehiasarian, U. Helmersson, J. Vac. Sci. Technol. A 23 (2005) 18.
[16] K. Bobzin, N. Bagcivan, P. Immich, S. Bolz, J. Alami, R. Cremer, J. Mater. Process. Technol. 209 (2009) 165.
[17] U. Helmersson, M. Lattemann, J. Bohlmark, A.P. Ehiasarian, J.T. Gudmundsson, Thin Solid Films 513 (2006) 1.
[18] M. Samuelsson, D. Lundin, J. Jensen, M.A. Raadu, J.T. Gudmundsson, U. Helmersson, Surf. Coat. Technol. 205 (2010) 591.
[19] G. Greczynski, J. Lu, M.P. Johansson, J. Jensen, I. Petrov, J.E. Greene, L. Hultman, Surf. Coat. Technol. 206 (2012) 4202.
[20] X. Tian, Z. Wu, J. Shi, X. Li, C. Gong, S. Yang, China Vac. 47 (2010) 44.
[21] S.K. Kim, B.C. Cha, Surf. Coat. Technol. 188–189 (2004) 174.
[22] NIST X-ray Photoelectron Spectroscopy Database, Version 3.3, National Institute of Standards and Technology, USA, 2003.
[23] http://www.lasurface.com/database.
[24] S. Zhou, L. Wang, Q. Xue, Surf. Coat. Technol. 206 (2012) 2698.
[25] K.C. Wong, X. Lu, J. Cotter, D.T. Eadie, P.C. Wong, K.A.R. Mitchell, Wear 264 (2008) 526.
[26] X.Z. Ding, X.T. Zeng, X.Y. He, Z. Chen, Surf. Coat. Technol. 205 (2010) 224.
[27] A.F. Yetim, I. Efeoglu, A. Celik, A. Alsaran, I. Kaymaz, J. Adhes. Sci. Technol. 25 (2011) 1497.
[28] B. Podgornik, Surf. Coat. Technol. 146–147 (2001) 318.
[29] F. Bidev, Ö. Baran, E. Arslan, Y. Totik, İ. Efeoğlu, Surf. Coat. Technol. 215 (2013) 266.
[30] K. Holmberg, A. Matthews, in: D. Dowson (Ed.), Coatings Tribology: Properties, Techniques and Applications in Surface Engineering, 1994.
[31] E. Arslan, F. Bülbül, A. Alsaran, A. Celik, I. Efeoglu, Wear 259 (2005) 814.
[32] S. Gangopadhyay, R. Acharya, A.K. Chattopadhyay, S. Paul, Vacuum 84 (2010) 843.
[33] D.G. Teer, J. Hampshire, V. Fox, V. Bellido-Gonzalez, Surf. Coat. Technol. 94–95 (1997) 572.